

Penetration Loss at 60 GHz for Indoor-to-Indoor and Outdoor-to-Indoor Mobile Scenarios*

Sung Yun Jun¹, Derek Caudill¹, Jack Chuang², Peter B. Papazian², Anuraag Bodi², Camillo Gentile², Jelena Senic², Nada Golmie²

¹ RF Technology Division, National Institute of Standards and Technology, Boulder, CO, USA, sungyun.jun@nist.gov

² Wireless Networks Division, National Institute of Standards and Technology, Gaithersburg, MD, USA,

* Publication of the United States government, not subject to copyright in the U.S.

Abstract—This paper investigates the penetration loss of an office building in indoor-to-indoor (I2I) and outdoor-to-indoor (O2I) mobile scenarios. The measurements were collected using our 60 GHz double-directional switched-antenna channel sounder. During measurements, the transmitter, mounted on a tripod, was placed in an office and outside of the building, while the receiver, mounted on a mobile robot, moved along an interior hallway. The penetration loss for a variety of building materials was predicted versus incident angle by electromagnetic propagation theory using the International Telecommunication Union Radiocommunication Sector (ITU-R) Recommendation P.2040 model parameters and compared with the measurement results. The wooden door, plasterboard wall, and interior glass were observed to have penetration losses ranging from 25.5 dB to 40.5 dB, 11.8 dB to 31.6 dB, and 7.5 dB to 18.1 dB, respectively, while the exterior building materials exhibited even larger penetration losses, ranging from 31.1 dB to 66.5 dB.

Index Terms—channel sounder, channel propagation model, 5G wireless communications, millimeter wave

I. INTRODUCTION

Fifth generation (5G) wireless communications have created a growing demand for millimeter-wave (mmWave) channel sounding and modeling. The modeling and optimization of 5G cellular network technologies are highly dependent on the radio-wave propagation characteristics [1]. mmWave communications will operate below ideal capacity in non-line-of-sight conditions as a result of the properties of the obstructing materials that cause attenuation due to absorption and dispersion of the electromagnetic waves.

To date, several studies have been conducted to measure the signal attenuation of materials at mmWave frequencies and to model path loss in indoor and outdoor environments: Extensive measurements for the penetration loss of various materials at 28 GHz and 73 GHz in an indoor office environment were studied in [2]-[3]. An experimental investigation of a 60 GHz wireless local-area network system in an indoor cubicle environment was performed in [4]; the measurement campaigns were conducted using horn antennas at fixed points within an indoor environment; the study resulted in an empirical O2I building model for penetration loss. Analysis of reflection and penetration losses for common building materials at 28 GHz was presented in an urban outdoor environment [5]. The suburban residential neighborhood penetration loss at 28 GHz was also investigated in [6]. Wideband channel measurements in

downtown Denver, CO at 9.6 GHz, 28.8 GHz and 57.6 GHz were collected in [7]; significant penetration loss was found to be caused by obstruction from an office building.

In general, previous literature dealing with penetration loss measurements has focused on stationary points using directional horn antennas with limited scan angles. Lacking to date is the effect on penetration loss of different points of incidence and different angles of incidence across the surface of building materials, to capture what a real communications system would experience during operation. To fill that void, this paper presents measured penetration loss at mmWave using an electronically switched double-directional channel sounder that was developed by the National Institute of Standards and Technology (NIST) [8]. The sounder has at the center frequency of 60.5 GHz: 2 GHz bandwidth, wide scan angle, and a mobile robot positioning platform. The measurement campaign was conducted in I2I and O2I environments. For the purpose of comparison, a theoretical analysis for the penetration loss of the building materials and its dependence on incident angle was also conducted.

The paper is organized as follows: The theoretical analysis and measurement setup are presented in Section II and Section III, respectively. Analysis of the penetration loss measurement results are described in Section IV, followed by conclusions in Section V.

II. THEORETICAL ANALYSIS

Radio propagation at an interface with dielectric materials will depend on a number of parameters, most importantly the center frequency of the signal, the angle of incidence of the signal with the interface, and the material properties themselves. Generally speaking, transmission through materials degrade at higher frequencies, at shallower angles, and for denser materials. In order to provide a benchmark for comparison with our ensuing measurements, we first conducted a theoretical analysis of penetration loss by means of the Fresnel equations [9], which provide the reflection and transmission coefficients of electromagnetic waves incident on a flat surface. The material properties are represented through a complex relative permittivity η , expressed through real and imaginary components as

$$\eta = \eta' - j\eta'' \quad (1)$$

TABLE I. MATERIAL PROPERTIES AT 60.5 GHz

Material Class	Real part of relative permittivity (η')	Imaginary part of relative permittivity (η'')
Air	1	0
Metal	1	2.9719×10^6
Wood	1.99	0.1135
Plasterboard	2.94	0.0628
Glass	6.27	0.1703

The values of the frequency-dependent components were accordingly set to the center frequency of our channel sounder.

Table I shows the complex relative permittivity of several common construction materials at 60.5 GHz per the ITU-R Recommendation P.2040 [10]. We focused our theoretical analysis on wood, glass, and plasterboard only, the dominant materials in the environment where the measurements were collected. The thickness of the single-layered wood and glass materials was set as 45 mm and 9.5 mm, respectively, to match properties of the office building under investigation; the multi-layered wall, rather, was set to 12.7 mm for the two plasterboard sheets separated by an air pocket of 88.9 mm; in reality, as observed through the measurements, there were also metal studs in between the sheets.

Fig. 1 shows the theoretical attenuation of the three materials versus incident angle from 0° to 85° . The attenuation grows exponentially with incident angle. The wood and glass have attenuation in the range from 20.1 dB to 38.7 dB and from 5.8 dB to 19.9 dB, respectively. On the other hand, the multi-layer plasterboard attenuation varied from 5.5 dB to 32.3 dB over the same angle range. Interestingly, the ripple observed in the attenuation of the plasterboard can be traced to the multi-layered structure.

III. MEASUREMENTS

This section describes the channel sounder and the measurement campaign used to collect data for the I2I and O2I mobile scenarios.

A. Channel Sounder

Our 60 GHz double-directional switched array channel sounder is described in detail in [8]. The correlation-based system utilizes a pseudo-random noise (PN) sequence as the probing signal. For increased dynamic range to deal with greater range and greater penetration loss, a longer PN sequence of 32767 chips with chip rate of 2 Gbits/s was employed for the I2I scenario and the O2I scenario (at the expense of channel sweep time).

The transmitter (TX) is comprised of an intermediate frequency (IF) section, a radio frequency (RF) up-conversion section, and an eight-element antenna array with a switching multiplexer (MUX) (see Fig. 2(a,b)). The receiver (RX) contains an analog-to-digital converter section, an RF down-conversion section, and a sixteen-element antenna array with

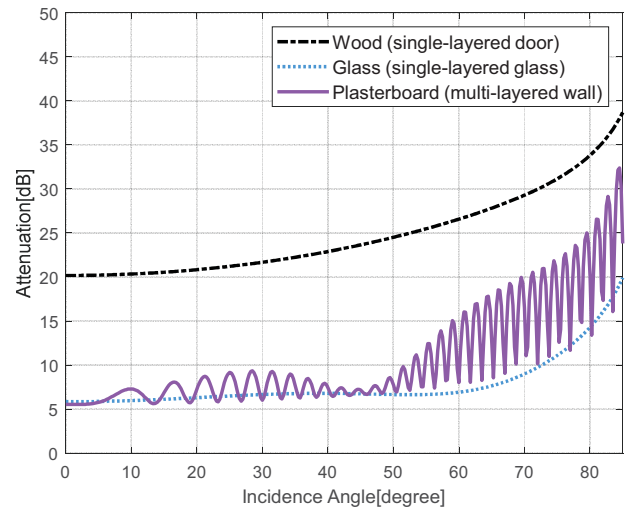


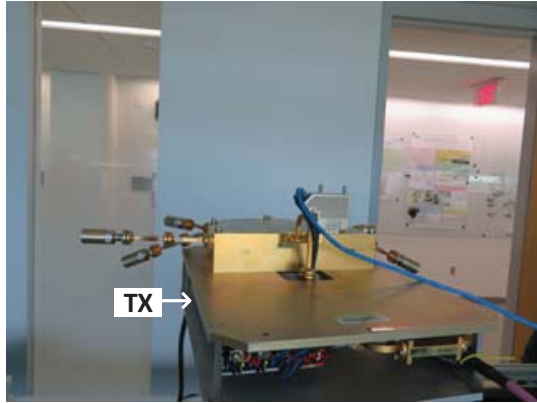
Fig. 1. Calculated transmission attenuation versus incidence angle for Wood, Plasterboard and Glass at 60.5 GHz.

a MUX (see Fig. 2(c,d)). Both arrays contain scalar feed horns with 18.1 dBi gain and half-power beamwidth of 22.5° . Given the constellation of the elements, the synthesized antenna patterns of the TX and RX arrays provide 180° and 360° field-of-view (FoV), respectively, in the azimuthal plane whereas the FoV in the elevation plane is 45° for both.

Two 10 MHz Rubidium time standards and timing control circuits are used for untethered timing synchronization between the TX and RX for switching transmission and reception of the PN sequences between the $8 \times 16 = 128$ channels. An arbitrary waveform generator (AWG) at the TX generates the PN sequence, which is modulated using Binary Phase Shift Keying at an IF frequency of 3 GHz and then up-converted to an RF frequency of precisely 60.5 GHz. The TX antenna array transmits the RF signal with an equivalent isotropic radiated power (EIRP) of 36 dBm. The received signal at the RX antenna array is then down-converted to the IF of 3 GHz and is digitized at 40 Gsamples/s per channel. Matched filtering of the digitized signal with the PN sequence to generate the channel impulse response for each TX-RX antenna pair is performed off-line to decrease the channel sweep time. The resultant data for one TX-RX measurement point therefore consists of 128 channel impulse responses.

To remove the systematic distortion effects caused by the system hardware, a back-to-back calibration method was applied, as described in [8]. The calibration significantly reduces distortions and internal reflections of the system, extending the dynamic range to 90 dB for the longer PN sequence. The antenna patterns of the directional horns were characterized in an anechoic environment and de-embedded from the measurements as part of the calibration procedures. The 128 channel impulse responses recorded are post-processed through the Space Alternating Generalized Expectation maximization (SAGE) algorithm [11] to extract the channel multipath components (MPCs) and their properties, namely the delay, angle-of-departure (AoD) and angle-of-arrival (AoA) (in both azimuth and elevation), and

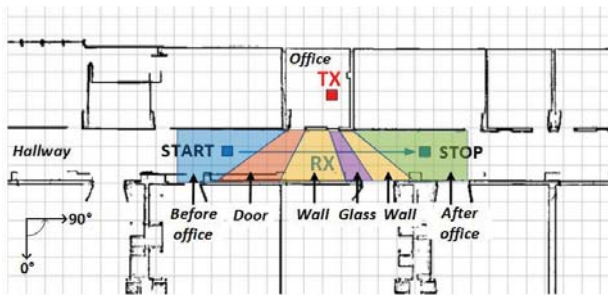
I2I Scenario



(a)



(c)

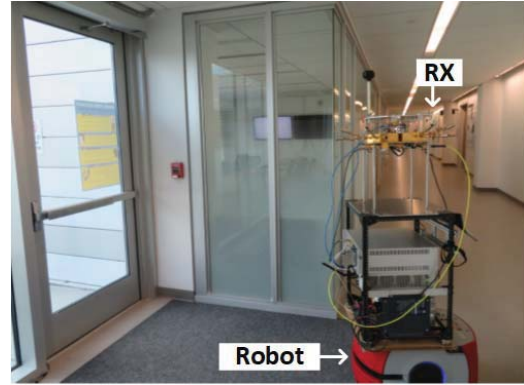


(e)

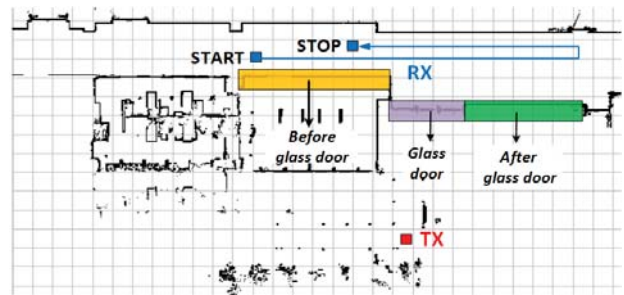
O2I Scenario



(b)



(d)



(f)

Fig. 2. Measurement setups for the I2I (left column) and O2I (right column) mobile scenarios. (a,b) TX positions (c,d) RX positions (e,f) Maps.

the path loss of each path identified. The aforementioned calibration procedures ensured that the features of the channel sounder were decoupled from the measurements such that properties of the extracted MPCs reflected the channel alone (and not the system).

B. Measurement Setup

The environment for the measurement campaign was a modern office building on the campus of the NIST in Boulder, CO, USA. Fig. 2(a,c) and Fig. 2(b,d) display photographs of the measurement setups for the I2I and O2I scenarios, respectively, and Fig. 2(e,f) show their maps. The maps were

automatically generated by the laser-guided navigational system of the robot, furnishing precision localization to within a centimeter. For the I2I scenario, the fixed TX was mounted on a tripod inside an office at height 1.6 m and facing the adjacent hallway; the RX, mounted on a mobile robot, traversed the route shown in Fig. 2(e) from start to stop in the hallway, over which 57 data points were collected within the TX-RX distance range of 2.7 m to 6.1 m. For the O2I scenario, the TX was raised to 2.5 m and placed outside the building, still facing the hallway; the RX traversed a longer route in the same hallway, shown in Fig. 2(f), over which 93 data points were collected within the distance range of 9.4 m to 13.7 m. For both scenarios, the direct path between the TX and RX was obstructed by single- and multiple-layered materials.

IV. MEASUREMENT RESULTS

The penetration loss for each measurement point collected was computed as in [3]: First, the *penetrating path* was identified among all MPCs extracted per measurement point as the one that arrived first. Its delay (τ) was then mapped to the theoretical free-space path loss (PL_{FS}) through Friis transmission equation as

$$PL_{FS} = 20 \cdot \log_{10} \left(\frac{4\pi c\tau}{\lambda} \right), \quad (2)$$

where c is the speed of light and $\lambda = 5$ mm is the wavelength corresponding to 60.5 GHz. Finally, the penetration loss was estimated by subtracting PL_{FS} from the measured path loss of the penetrating path. In the sequel, we present the estimated penetration loss for the I2I and O2I scenarios.

A. I2I Penetration Loss

For the purpose of verification, Fig. 3 displays the estimated delay, AoA, and path loss of the penetrating path (dashed red) versus the position index of the I2I scenario. Also displayed are the analogous theoretical values for the free-space direct path (solid blue), where its delay (τ_{DP}) and AoA were computed from the geometry of the known TX and RX positions and direct path loss (PL_{DP}) was computed by substituting τ_{DP} into (2). Aside from any system estimation error, the reason the estimated delay / AoA differ from the theoretical values is because the trajectory of the penetrating MPC deviated from the direct path due to reflection, refraction, and dispersion occurring at the material boundaries and/or in the environment; the difference in path loss, rather, is equivalent to the estimated penetration loss. Note that in general the deviation in delay / AoA increased with penetration loss.

In order to classify the estimated penetration loss according to the dominant materials in the environment, we partitioned the side of the hallway penetrated by the signal into *zones*; the partitioning was based on where the theoretical direct path intersected the side as the RX moved in the hallway. Fig. 2(e) displays the resultant partitioning with different colors: For the single penetration from the office, the side was constructed from a wooden door, plasterboard and glass sections; the measured penetration loss there ranged from 25.5 dB to 40.5 dB, from 11.8 dB to 31.6 dB, and from 7.5 dB to 18.1 dB, respectively. For the segments before and after the office, on the other hand, the side was constructed totally from plasterboard, through which multiple penetrations (including the adjacent vertical office walls) occurred; there the penetration loss increased in range from 34.4 dB to 40.5 dB and from 26.0 dB and 47.6 dB, respectively, as shown in Fig. 4(a). The interior glass featured the lowest penetration loss among the environment materials.

The penetration loss of the wooden door, plasterboard wall, and interior glass were slightly higher than the attenuation characteristics of the ITU-R P.2040 model (Fig. 1). It was determined that the door is made of fire-rated wood with a composite mineral core containing several different

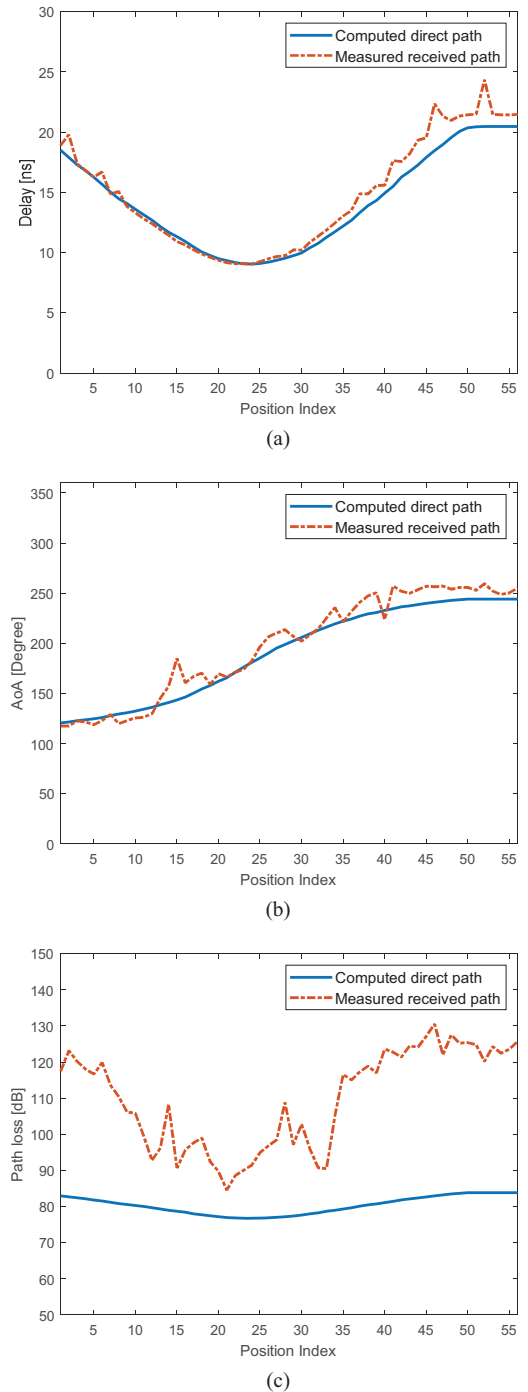


Fig. 3. Properties of the penetrating path identified from the I2I measurement versus the theoretical properties of the direct path. (a) delay (b) AoA and (c) path loss.

materials. The composite materials have more complex reflection and transmission effects, which cause the high attenuation versus the homogenous materials. Moreover, the multiple peaks of the penetration loss in the wall can be explained by the metal studs installed at regular spacing between the plasterboard sheets. The thin window film on the glass (for privacy) also provides a slightly higher penetration loss compared to clear glass (Fig. 1).

B. O2I Penetration Loss

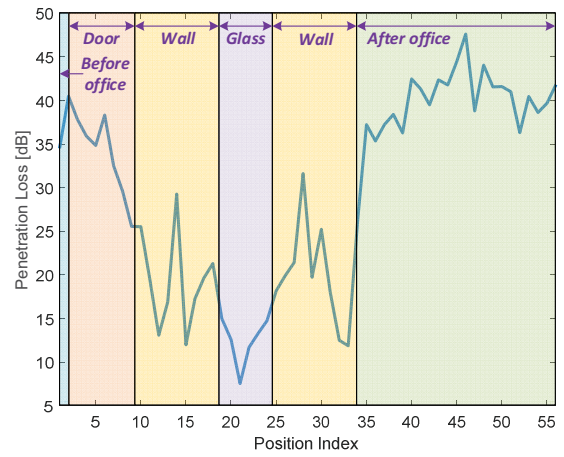
Fig. 2(f) displays how the side of the hallway penetrated by the signal was partitioned based on the exterior construction materials for the O2I scenario, and Fig. 4(b) displays the corresponding results for the penetration loss estimated. Along the segment before the glass door with double-pane glass, there is the conference room between the TX and RX for which the penetrating path most likely went through an exterior double-pane window to the conference room and then out a single-pane interior window to the hallway. The exterior window consisted of a single, clear inner glass pane and a single, tinted outer glass pane separated by 19 mm (the outer pane tint had low emissivity coating applied to reject ultraviolet light). The interior windows were clear single pane glass. The segment after the glass door was an exterior wall. The segments before and after the glass door exhibited huge penetration losses, ranging between 52.3 dB to 66.5 dB and 40.3 dB to 59.2 dB, respectively. On the other hand, the glass door had a penetration loss in the range of 31.1 dB to 46.0 dB with an average value of 38.5 dB. It was observed that external building materials such as metal plating and low emissivity coatings caused high attenuation.

V. CONCLUSION

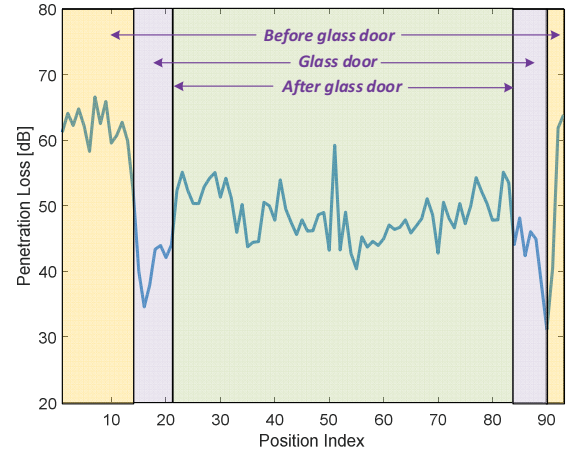
This paper presents measurements for penetration loss taken with our 60 GHz channel sounder over a variety of building materials in I2I and O2I mobile scenarios. Departing from previous efforts, the penetration loss was measured across continuous incident points and, by association, different incident angles along the surface of the building materials in the environment, to capture what an actual radio would experience in motion as opposed to a collection of separate, fixed-position measurements. As a means for comparison, the penetration loss for the building materials in the environment were modeled and analyzed theoretically through the Fresnel equations fit with the ITU-R P.2040 material parameters. The penetration loss through multiple layers was observed to be as high as 47.6 dB for I2I scenario, yet not as high as the 66.5 dB observed for the O2I scenario. In summary, we conclude that signals transmitted at 60 GHz both inside buildings and into buildings will suffer from severe penetration losses due to ambient building materials, heavily reducing coverage with respect to line-of-sight conditions. On the other hand, the high penetration loss of building materials can be a potential advantage to reduce interference from neighboring wireless network systems.

REFERENCES

- [1] K. A. Remley et al., "Measurement Challenges for 5G and Beyond: An Update from the National Institute of Standards and Technology," *IEEE Microwave Mag.*, vol. 18, no. 5, July–Aug. 2017, pp. 41–56.
- [2] M. Lei, J. Zhang, T. Lei, and D. Du, "28-GHz indoor channel measurements and analysis of propagation characteristics," *Proc. IEEE Int. Symp. Personal, Indoor and Mobile Radio Commun. (PIMRC)*, 2014, pp. 208–212.
- [3] Ryan, J., MacCartney, G. R., and Rappaport, T., "Indoor Office Wideband Penetration Loss Measurements at 73 GHz," *IEEE International Conference on Communications Workshop (ICCW)*, pp.1-6, Paris, France, May 2017.



(a)



(b)

Fig. 4. Measured penetration loss for (a) I2I and (b) O2I scenarios.

- [4] A. Maltsev, R. Maslennikov, A. Sevastyanov, A. Khoryaev, and A. Lomayev, "Experimental investigations of 60 GHz WLAN systems in office environment," *IEEE J. Sel. Areas Commun.*, vol. 27, no. 8, pp. 1488–1499, Oct. 2009.
- [5] H. Zhao et al., "28 GHz millimeter wave cellular communication measurements for reflection and penetration loss in and around buildings in New York City," *Proc. IEEE Int. Conf. Commun. (ICC)*, Jun. 2013, pp. 5163–5167.
- [6] J. Du, D. Chizhik, R. Feick, G. Castro, M. Rodríguez and R. A. Valenzuela, "Suburban residential building penetration loss at 28 GHz for fixed wireless access," *IEEE Wireless Commun. Lett.*, vol. 7, no. 6, pp. 890–893, Dec. 2018.
- [7] E. J. Violette et al., "Millimeter-wave propagation at street level in an urban environment," *IEEE Trans. Geosci. Remote Sens.*, vol. 26, no. 3, pp. 368–380, 1988.
- [8] R. Sun, P. B. Papazian, J. Senic, Y. Lo, J.-K. Choi, K. A. Remley, and C. Gentile, "Design and calibration of a double-directional 60 GHz channel sounder for multipath component tracking," *Proc. IEEE European Conf. Antennas and Propagation*, pp. 1–5, Mar. 2017.
- [9] J. Medbo and S. Dwivedi, "Frequency Selectivity of Window Attenuation up to 100 GHz," *2019 13th European Conference on Antennas and Propagation (EuCAP)*, Krakow, Poland, 2019, pp. 1-4.
- [10] Recommendation ITU-R P.2040, "Effects of building materials and structures on radiowave propagation above about 100 MHz," <https://www.itu.int/rec/R-REC-P.2040-1-201507-1/en.I.S.>
- [11] J. A. Fessler and A. O. Hero, "Space-alternating generalized expectation-maximization algorithm," *IEEE Trans. Signal Process.*, vol. 42, no. 10, pp. 2664–2677, Oct. 1994.